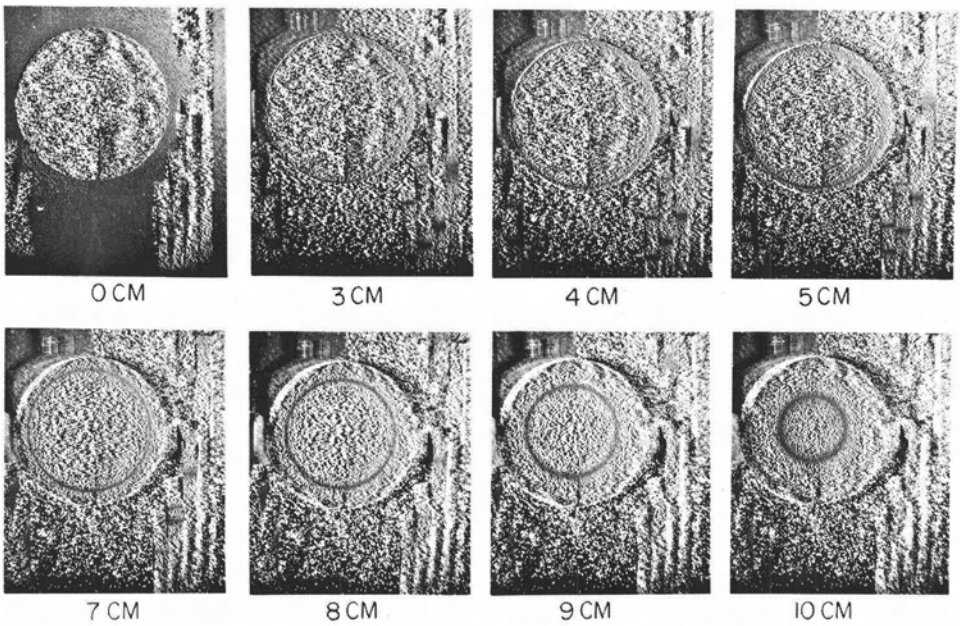

FRONTISPIECE. Example output from the Positive-Negative system with incoherent illumination. The successive gray circles are contour lines of a hemisphere (Figure 3) at the indicated contour intervals. The successive prints were made from the same pair of negatives by simply adjusting the x-displacement.

DR. ALAN WERTHEIMER*
DR. M. PARKER GIVENS
University of Rochester
Rochester, N.Y. 14627

Rapid Contour Generation

Two optical processing systems have certain advantages which accrue from the extremely rapid extraction of contour information without the need for stereo perception, electro-optical scanning systems, or computers.

(Abstract on next page)

INTRODUCTION

MUCH INTEREST has been expressed in the past several years in the development of automated methods of extracting information from stereoscopic photographs. Advances in this area have come primarily from applications of computer technology and electronic correlation systems, many of which are described in DiPentima's review article.[1] To this date, however, relatively little work has been done in the area of locating elevation contours entirely by optical processing techniques.

*Dr. Wertheimer is now affiliated with Leeds & Northop Co., North Wales, Pa. 19454.

Work with incoherent illumination was done by Goldfischer and Vesper[2], whereas Real[3] suggested some applications utilizing coherent optical techniques. Bendix Corporation has made several advances, using both electro-optical systems and coherent optical processing systems.[4,5,6] Still, most automated contour extraction systems require sequential scanning of the input imagery. Thus, whether the scan is converted to an electrical signal or remains an optical light beam during the procedure of image matching, the processing is done in a point-by-point manner. Two exceptions are the Bendix *Instant Profile* correlator[5] which processes a thin strip of imagery, and the Bendix *Con-*

ABSTRACT: *Two optical processing systems for rapid contour generation from vertical transparencies include: the Positive-Negative system that uses transparencies processed to plus and minus values of gamma, and produces dark contours on a structure filled background; and the Scatter-Plate system in which matching imagery produces bright contour bands on a dark field. For a given x-parallax setting all contours are displayed simultaneously. Experimental work treats close-range photogrammetric examples. Mathematical and experimental methods provide a determination of the height discrimination.*

tour-Hypsocline Generator[6] which, for a specific parallax setting, processes the entire image field.

This paper presents several new techniques for the simultaneous display of all contours at a particular elevation by use of optical processing systems. The contours may be viewed directly or recorded photographically, as desired. The output from these systems does not compete with the high accuracy attainable with classical stereoplotting techniques. The advantages, rather, come from the extremely rapid extraction of contour information without the need for stereoscopic perception, electro-optical scanning systems, or electronic computers.

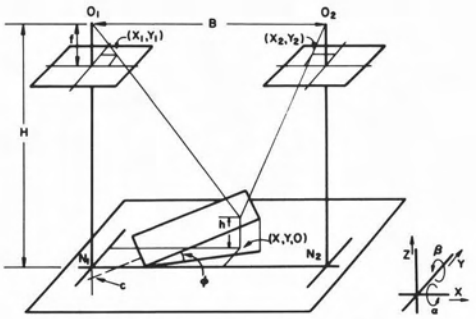

FIG. 1. Vertical model with sloping terrain.

THE VERTICAL MODEL

The optical processing systems described here currently require input transparencies that are taken vertically, or have been rectified to a vertical orientation. Figure 1 provides a diagram for the vertical case. The photos, shown as contact transparencies of the original negatives, are on the object side of the perspective centers O_1 and O_2. The principal distance f is the same for both photographs. The optical axes O_1N_1 and O_2N_2 are separated by the base B and are perpendicular to the reference plane, that is at a distance H from the perspective centers.

The height from the reference plane h and the ground coordinates X and Y of a point in the object space are determined from the photo coordinates of the images of that point. Defining X and Y to be zero where the O_1N_1-axis intersects the reference plane, the equations are:

$$h = H - fB/p \tag{1}$$

$$p = x_1 - x_2 \tag{2}$$

where

$$X = x_1[(H-h)/f]; \; Y = y_1[(H-h)/f]. \tag{3}$$

It is useful, here, to consider the perspective distortion which occurs in viewing sloping terrain from different camera stations. For terrain with a constant slope, as shown in Figure 1, closed-form equations exist to describe a region of imagery in the x_2, y_2 plane, in terms of the conjugate imagery in the x_1,y_1 plane. The coordinate axes to the right of the main diagram show the sign conventions with all parameters on the small diagram positive as drawn.

The ramp, if extended, intersects the optical axis O_1N_1 at c, which is negative if below the reference plane as shown. An ordered rotation, first α about the x-axis, then β about the y-axis, produces a ramp which makes an angle of ϕ with respect to the reference plane. The sign of the rotation is positive if an increase in height occurs as one moves in a positive axis direction. For example, the first rotation α is positive if movement in the $+y$-direction causes motion *up* the ramp.

Writing the x_2 coordinate of a point of imagery in terms of its x_1 coordinate, and eliminating X and Y, yields:

$$x_2 = x_1 - p_0 - p(x_1, y_1) \tag{4}$$

where

$$p(x_1,y_1) = \epsilon_x(x_1 - x_0) + \epsilon_y(y_1 - y_0) \tag{5}$$

and

$$\epsilon_x = \frac{B\tan\beta}{(H-c)\cos\alpha}, \quad \epsilon_y = \frac{B\tan\alpha}{(H-c)} \tag{6}$$

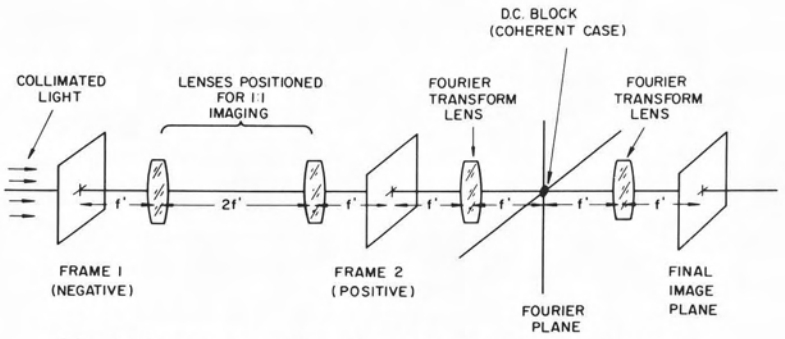

FIG. 2. The optical configuration of the Positive-Negative system.

The constant p_0 is the x-parallax shift required to bring matching imagery into exact coincidence at $x = x_0$ and $y = y_0$, if one transparency is placed on top of the other.

Due to the absence of y-parallax the y_1 and y_2 coordinates of the matching imagery are equal. Thus, after the appropriate x-shift the transmission of the first transparency is written in terms of the second as

$$T_1(x_1, y_1) = T_2\left[x_1 - p(x_1, y_1), y_1\right]. \quad (7)$$

This perspective distortion described by Equation 7 will define the width of the contours produced by these systems for a constant terrain slope. As most objects can reasonably be broken into suitably small regions over which the slope is fairly constant, the simple ramp model gives great insight into the system performance for more complex shapes. Finally, it can be shown that

$$tan^2\phi = \left[tan^2\alpha + tan^2\beta/cos^2\alpha\right]. \quad (8)$$

THE POSITIVE-NEGATIVE SYSTEM

The first basic system, the positive-negative contour generator, is essentially a selective masking technique.[7] Starting with two vertical photographs, a contact transparency is made of one and developed to a unit gamma. Alternately, contact transparencies are made from both, and the processing done so that the gammas are equal in magnitude but opposite in sign. An optical system now images the first copy onto the second, with unit magnification, as shown in the left half of Figure 2. Projecting one transparency through the other results in the multiplication of the individual intensity transmissions, or equivalently, the summation of the individual transmission densities. The analysis, here, is done in terms of density addition.

The contact copying process assumes that the log-exposure range is within the linear region of the density *vs.* log-exposure curve, so the copy density is represented[8] by

$$D(x,y) = \gamma log\, E(x, y) - D_o. \quad (9)$$

Here, γ is the slope of the straight line portion of the curve, and $-D_o$ is the intersection of the straight line portion extended to cross the density axis. The log-exposure $E(x,y)$ is equal to the log-intensity (a constant) minus the density of the original transparency being copied. Combining constants yields:

$$D_a(x, y) = D_{oa} - \gamma_a D_1(x_1,y_1)$$
$$D_b(x, y) = D_{ob} - \gamma_b D_2(x_2, y_2). \quad (10)$$

The constants D_{oa} and D_{ob} represent the densities on the respective copies that would result if the original transparency had a density of zero.

The summation of densities is now written with the general approach used for Equation 7. Using the Equations 10 with $\gamma_a = -\gamma_b = \gamma$ and, dropping the subscripts from x_1 and y_1, produces

$$D(x,y) = D_{oa} + D_{ob} + \gamma\left[D_2(x,y) - D_2(x - p(x,y), y)\right]. \quad (11)$$

Finally, if $p(x, y) = 0$ over a small region, the final term in Equation 11 goes to zero. The density over this region is, therefore, constant. Visually, the isolation of this region of uniform intensity depends on the contrast between the region and the structure of the surrounding, slightly mismatched area.

INCOHERENT OPERATION

To demonstrate the performance of this system, a laboratory model was constructed, as shown in Figure 3 consisting of a hemisphere of 10.8 cm radius, and several ramps of varying slopes, approximately 7 to 8 cm in height. Circular features of two sizes, sprinkled on different portions of the model, provided the detail. Photographs were taken from several positions along a line 108.6 cm above the base of the model, using a 35-mm camera with a 50-mm focal length Nikon en-

larging lens. The lens was chosen for its relatively low distortion characteristics. The two photographs used here overlapped the central and right hand portion of the model with a stereo base of 19.0 cm. The principal distance f was 5.24 cm.

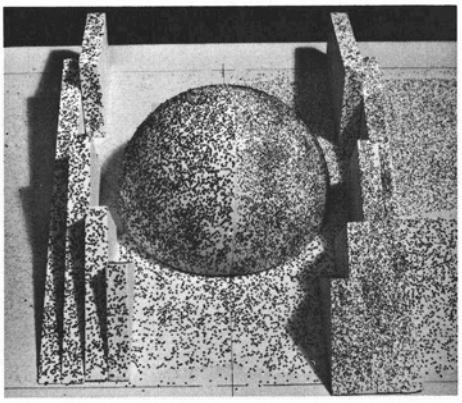

FIG. 3. The laboratory model.

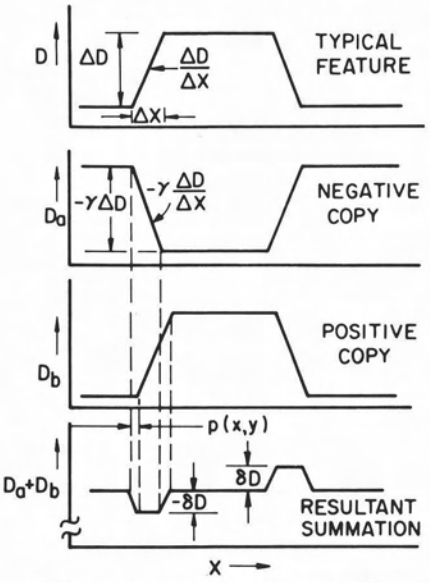

FIG. 4. System performance for slightly mismatched imagery.

Frame 1, as shown in Figure 2, was an original negative, whereas Frame 2 was a positive transparency made from the other negative. This positive contact was made on Kodak 5302 Fine-Grain Release Positive film, and developed in D-76 to a gamma of 1.0. Frame 1 remained fixed, whereas Frame 2 was moved laterally across the image of Frame 1 to correspond to different x-parallax values. With incoherent illumination, the two Fourier transform lenses served merely to relay the product image to the final image plane where recordings were made on film.

The Frontispiece contains a partial set of photos recorded at parallax settings representing 1-cm contour intervals. Incoherent illumination was used for this series of photographs. The ramps in the right hand portion of each photograph are useful for evaluating the system accuracy as a function of terrain slope, whereas the hemisphere provides a surface which yields continuous contour bands.

The visualized width of a contour band depends, among other things, on how rapidly $p(x,y)$ changes from zero (its value at the point of perfect image coincidence), and how rapidly the resultant density summation in Equation 11 changes for a particular value of $p(x,y)$. This second consideration is illustrated schematically in Figure 4. Microdensitometer traces have shown that the individual features can be approximated quite well by piecewise continuous functions as drawn. A typical rate of change of density $\Delta D/\Delta x$ on the original negatives is about 0.028 density units/micrometer, occurring over a distance, Δx, of roughly 25 μm. From this model, the density change, δD, as shown in Figure 4, for $|p(x,y)|$ less than 25 μm, is

$$\delta D = \gamma \frac{\Delta D}{\Delta x} p(x,y). \qquad (12)$$

The individual features in the immediate region of a contour band are completely matched at the contour center, and gradually become mismatched for elevations above and below the contour level. Completely mismatched features produce a total density range of $2\gamma\Delta D$ about the mean density $D_{oa} + D_{ob}$. This is seen by considering the situation of a large value of $p(x,y)$ in Figure 4. As a visual criteria for determining the edge of a contour band, one might require the density change in Equation 12 to be at least 20 percent of the maximum density fluctuations caused by substantially mismatched features, or

$$\delta D = 0.20\,(2\gamma\Delta D). \qquad (13)$$

To attain this value of δD, one goes from the contour center in a direction perpendicular to the contour line, until $p(x,y)$ is sufficient to cause the density change required by Equation 13. Consider, for simplicity, a terrain slope only in the Y-direction. Equations 5 and 6, then, with $\beta = O$, produce

$$p(x,y) = \frac{B \tan \alpha}{(H - c)} (y - y_0). \qquad (14)$$

The contour band, centered at y_0, has a half-

width of $|y - y_0|$ defined by combining the Equations 12 through 14.

$$y - y_0 = \frac{0.4\ \Delta D\ (H-c)}{B \tan\alpha\ (\Delta D/\Delta x)}. \qquad (15)$$

The full width w which is twice the half-width, $|y-y_0|$, relates to the contour elevation uncertainty, δh. This uncertainty, expressed as a percentage of the height H above the terrain, is calculated from the approximate relation,

$$\frac{\delta h}{H} = \frac{100w}{f} \frac{H}{(H-c)} \tan\alpha. \qquad (16)$$

Here, f, c, and H are as shown in Figure 1. Finally, substitution for w in the last equation produces:

$$\frac{\delta h}{H} = \frac{80\ H}{fB} \frac{\Delta D}{(\Delta D/\Delta x)}. \qquad (17)$$

It should be noted that, independent of the orientation of the terrain slope, the individual features will always be sheared in the x-direction as the imagery starts to go out of coincidence. Hence, the rate of density term, $\Delta D/\Delta x$, is always taken with respect to the x-direction. Ultimate system performance is limited by the sharpness of the edges of the features in the photographs, and it is the modulation transfer function of the film-lens combination that defines the edge sharpness of the final image for a given scene.

Implicit in this analysis is the requirement for sufficient structure on the object in the region of interest. If the image detail is very sparse or missing completely, there will be little or no contrasting structure to define the boundaries of the contour band. This situation is shown in the upper left corner of the photos in the Frontispiece, where there was no significant structure on the model, and hence a uniform region producing an apparent contour for all elevations.

The parameters used for the laboratory model and the microdensitometer traces of the imagery provided data which predicted a height uncertainty of 0.22 percent of the object distance, as calculated from Equation 17. To check this, contour band widths were measured with a filar eyepiece, viewing the output directly. (The average of several sets of data, expressed as the percentage height uncertainty $\delta h/H$ is shown later in Figure 12, with the measured values corresponding, roughly, to the calculated value for gentle slopes.)

The measured decrease in resolution with increased slope angle is primarily due to the fact that the number of individual circular features per unit area on the model is fairly constant. If the slope increases, $p(x,y)$ increases as the tangent of the angle, whereas the number of features per unit area of the image increases only as one over the cosine. Unless there are features present precisely at the point where $p(x,y)$ is large enough to produce the required minimum density fluctuations, the contour band will appear wider than it should be, and the height uncertainty will increase.

Coherent Operation

Considerable visual enhancement of the output is achieved by use of coherent illumination and simple optical processing techniques. As a contour band is a region in which the normal scene detail becomes washed out, one may consider that the amplitude transmission of this region consists only of a constant bias and some low spatial frequency terms. Under coherent illumination the spatial frequency components of the composite product are displayed in the Fourier plane, located as shown in Figure 2. A small opaque spot placed on the optical axis blocks the *D.C.* and very-low spatial frequency components from the entire scene, and passes the higher spatial frequency information on to the final image plane. Thus the intermediate intensity contour bands become dark bands, as shown in Figure 5, increasing their contrast with the surrounding area.

The *D.C.*-component removal for contrast enhancement introduces secondary effects which, in this system, tend further to enhance the contour definition. These effects occur because a coherent optical system operates linearly in amplitude, and this amplitude may take on positive and negative values. Removal of the *D.C.*-bias component from the entire scene means that the amplitude of any scene detail oscillating about this bias level, now oscillates about zero. If recorded photographically or viewed, however, one sees the intensity, the square of the amplitude, that is always greater than or equal to zero. This explains the apparent increase of bright detail in the background areas in Figure 5 as compared to Figure 3. Whereas the major advantage here is the increased visibility of the contours, there is also a slight narrowing of the measured contour widths due in part to the increased amount of bright detail.

High Contrast

Even though the gamma terms cancel in the expression for the height uncertainty in Equation 17, the photographic contrast of the

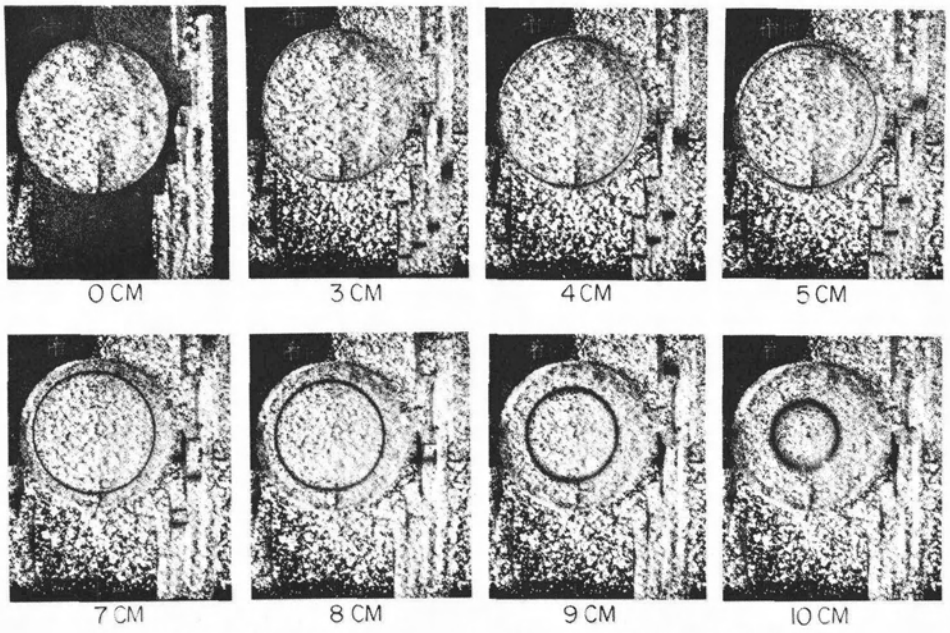

FIG. 5. The Positive-Negative system with coherent light and a *D.C.* block.

copying process has a great influence on the visibility of the contour bands. The average density $D_{oa} + D_{ob}$ (from Equation 11) increases as the gamma of the copying process increases. As this occurs, the contour bands become darker and more visible against the mismatched background detail. If this system is used with incoherent light, then, much better performance is attained with high-contrast copies. Coherent illumination and *D.C.* blocking still improves the performance, although not as dramatically as for the lower-contrast copies.

Figure 6 provides comparison photos for copies made with a gamma of 2.0. The left-hand photo was recorded with incoherent illumination, and shows a substantial improvement over the corresponding photo in the Frontispiece. The right-hand photo, shows a slight improvement over the left, but not as marked as between the Frontispiece and Figure 5. The copies used in the system were made on Kodak Process plates, after one negative was copied on 5302 film, as described earlier.

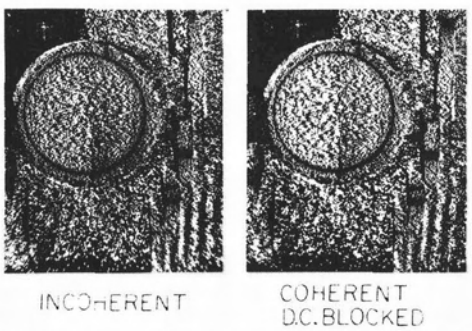

FIG. 6. Gamma of copying process equal to ± 2.

SCATTER-PLATE SYSTEM

The second basic system to be described is based on principles of the scatter-plate interferometer, described by Burch.[9] It is an in-line optical system with some similarities to the Bendix Coherent Optical Image-Image Correlator.[10] The optical system, shown in Figure 7, appears much like that of the positive-negative system, but the principles of operation are substantially different.

An outline of the mathematical treatment of this system is deferred to the appendix, but a non-technical explanation is fairly straightforward. Consider Figure 7 in which the first and second frames are identical. Collimated light is diffracted, or scattered, by the first transparency, and any light which is not scattered is removed by a *D.C.* block in the first Fourier plane. The scattered light, collected by the second lens, is directed towards the second transparency. There, due to the identical nature of the scene, the scattering or diffraction that occurs redirects much of the light into a collimated beam, as it was initially. The third lens focuses the collimated light through a tiny pinhole, and this suppresses any light which was not properly recollimated. Finally, the light is passed on to

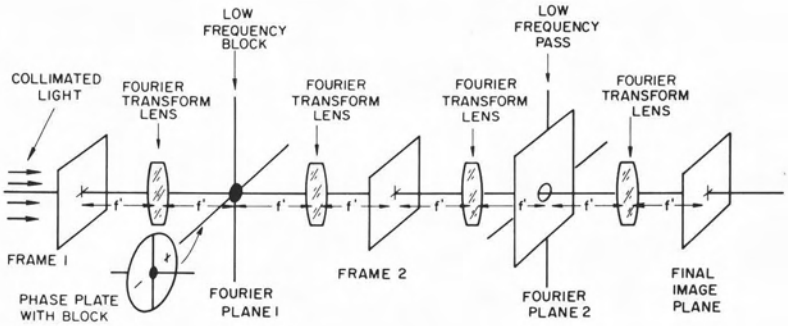

FIG. 7. Optical configuration of the Scatter-Plate system.

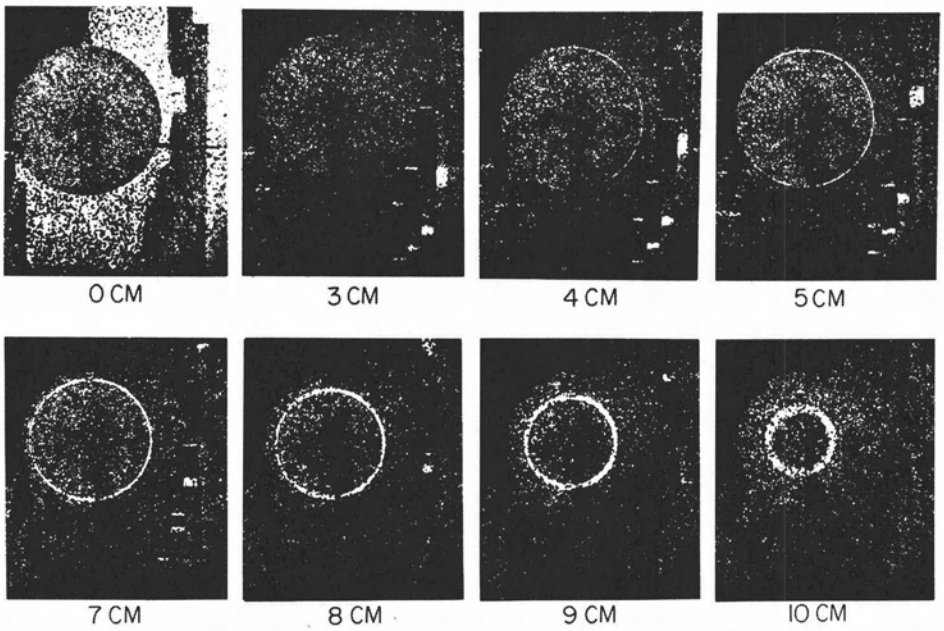

FIG. 8. Output from Scatter-Plate system.

cover the final image plane, indicating the area over which a match occurred.

In practice, only a small portion of the two transparencies match exactly. Therefore, the pinhole must be made larger to provide resolution of the matched areas in the final image plane, whereas the *D.C.* block must always be as large or larger than the pinhole. Mismatched areas, on the average do not produce the strong intensity characteristic of matched areas. Thus, the matched regions appear as bright contours on a much darker field.

To predict the actual contour widths, analysis is done in terms of the light amplitude, as discussed earlier, because this is a coherent system. The average value of the light amplitude, as outlined in the appendix, is

$$\overline{a(x,y)} = b_2(x,y) * \{[b_1(x,y)^* R(x,y)] \mid x = p(x,y),\ y = 0\} \tag{18}$$

where a is the light amplitude, b_1 and b_2 are the optical spread functions due to the block in the first Fourier plane and the aperture in the second Fourier plane, and $R(x,y)$ is the autocorrelation of the input scene in the region of the contour. The symbol * denotes a convolution. This expression is the statistical average for many samples, but not necessarily the exact value for a specific x and y location on a contour band. Statistical fluctuations occur about the average value and, in general, tend to increase as the aperture becomes larger. Unfortunately, making the aperture smaller to suppress these fluctuations to give the output a less noisy appear-

ance, has a widening affect on the contour width. Hence, a trade-off occurs between a narrow contour width and the suppression of noise.

Photographs of the output from this system appear in Figure 8. The imagery used for the first system is used again for comparison. The

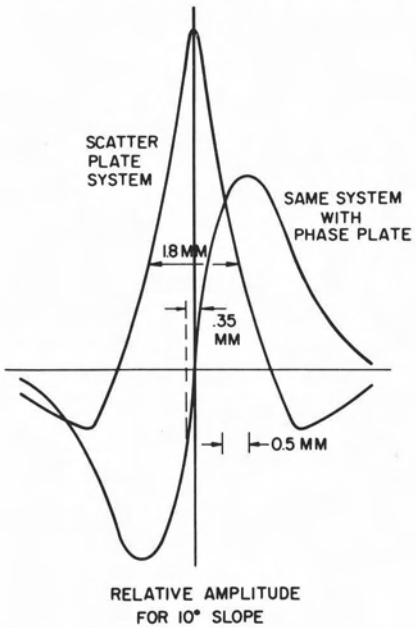

FIG. 9. Average amplitudes with widths drawn at 0.316 maximum amplitude.

block and aperture were both circular with equal diameters of 0.84 mm. Contour widths were measured visually as before, and the average of several sets of data appear later (in Figure 11). The contours, as seen by comparing Figures 5 and 8, are wider in this case.

Calculation of the predicted contour width from Equation 18 is made fairly easily in this instance, because the features in any region of the model were all circles of a specific size. They were spaced widely enough apart so the local autocorrelation was very close to that of a single circular feature. From Equation 18 the average amplitude was computed using the small features, which were 64 μm in diameter on the negatives. The higher of the two curves in Figure 9 shows this average value for a 10° slope, with a block and aperture as specified previously. As mentioned earlier, it is the intensity, or square of the amplitude that is seen. A reasonable visual criterion for defining the extent of the bright region is the requirement for a one-log unit drop in intensity before the boundary of the band is defined, and this is equivalent to a reduction to 0.316 of the maximum amplitude. With this criterion, the visualized contour width would be 1.8 mm on the negative, which, for the 10° slope, means an uncertainty of $\delta h = 0.6$ *percent*. H.

The measured values in Figure 11 agree well with this approach. Application of Equation 18 for steeper slopes shows that the nominal contour width is spread due to the effects of the final imaging aperture. The resulting increase in uncertainty, predicted by this equation, is confirmed by the measurements for steeper terrain.

Phase Plate

A substantial increase in sensitivity occurs with the use of a particular low-frequency block consisting of an opaque spot combined with a phase plate, as shown in Figure 7. A glass plate coated with a thin film of zinc sulfide is positioned in the first Fourier plane so that the boundary of this coating intersects the location of the *D.C.* component and is perpendicular to the direction of the x-parallax. The thickness of the film is such that the beam passing through one section of the filter is retarded by exactly one-half an optical wavelength from the beam traversing the other portion.

This filter, as calculated from Equation 18, causes the expected value of the amplitude to pass through zero at the center of the matched imagery. A curve for a 10° slope is shown in Figure 9 in comparison with the identical system without the phase plate. Due to the squaring of the amplitude, a typical contour band has a dark center outlined by bright borders on either side, as shown in the photos in Figure 10.

The phase plate generates significantly narrower contours, competitive with those of the positive-negative system. The criterion of a 1 log-unit drop from the maximum intensity predicts a contour width of 0.35 mm as measured from Figure 9, which corresponds to a height uncertainty of 0.12 percent. Visual measurements, plotted in Figure 11, confirm this expected improvement.

Certain problems occur with this configuration, however. For steep slopes the contour band intensity drops somewhat more than without the phase plate, so that contours on steep terrain become more difficult to locate. Alternately, for very broad flat areas, as in the first photo of Figure 10, the central dark fringe expands to cover the entire flat area. Without the bright border, one cannot distinguish the contour center from the background. Nevertheless, the gentle and intermediate slope performance is greatly improved with the addition of the phase plate.

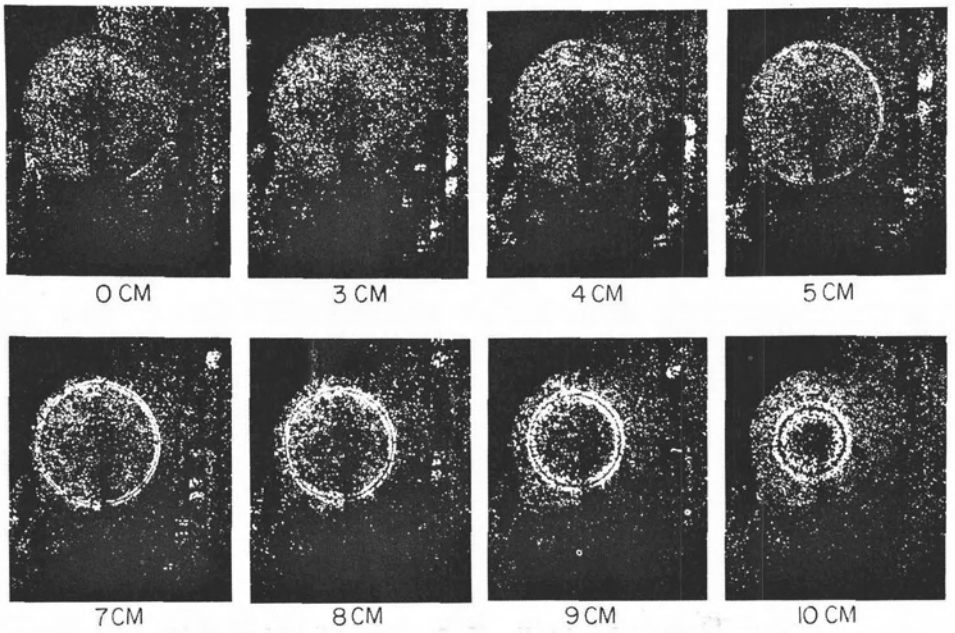

FIG. 10. The Scatter-Plate system with the phase plate inserted.

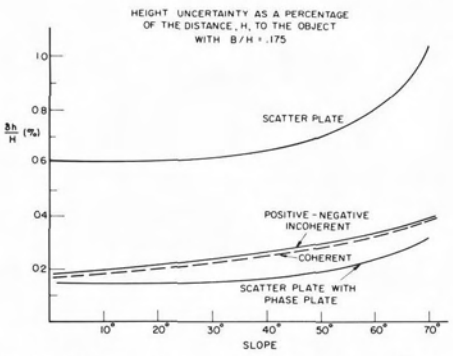

FIG. 11. Measured accuracy of the systems based on visually determined contour widths.

ACTUAL APPLICATION

The requirement for moderate- to high-contrast imagery in both these systems suggests they may be most useful for close-range work where control is attainable over the surface detail of the model, or over the illumination. As an example, an application is shown in which human body contours have been generated.

An image of a random-dot pattern, projected onto the back and shoulder area of a live model, provided the scene detail. Two 35-mm cameras, separated by 43.2 cm, and located 203 cm from a reference frame in the model area, took simultaneous left and right side views. Plus-X film was used as a compromise between exceptionally fine grain and rapid speed, and was slightly overdeveloped to increase the contrast. The photographic negatives were put directly into the processor in the scatter-plate/phase-plate mode. The block and aperture had diameters of 0.54 and 0.50 mm, respectively. Photographs were recorded for one cm contour intervals, and some of them are reproduced in Figure 12.

For comparison, the original input negatives were plotted by classical means using a Balplex 760 plotter. A reproduction of this plot is shown in the left half of Figure 13. The right half of that figure was constructed by reprojecting the negatives individually, and tracing the contours onto a common manuscript. What occurs to be about a one-quarter cm disparity between equivalent contours was due to an initial difficulty in establishing the reference level in the optical processors. This difficulty could have been avoided by a slight improvement in the control features.

GENERAL CONSIDERATIONS

One facet of these systems, in which the image matching is done on the surface of one of the transparencies, is that the contours generated are perspective contours rather than the required orthoscopic contours. However, a simple optical solution exists. As Equation 3 shows, the orthoscopic contour information is scaled from the coordinates of the imagery on the transparency. The scaling parameter (which is the same for all features

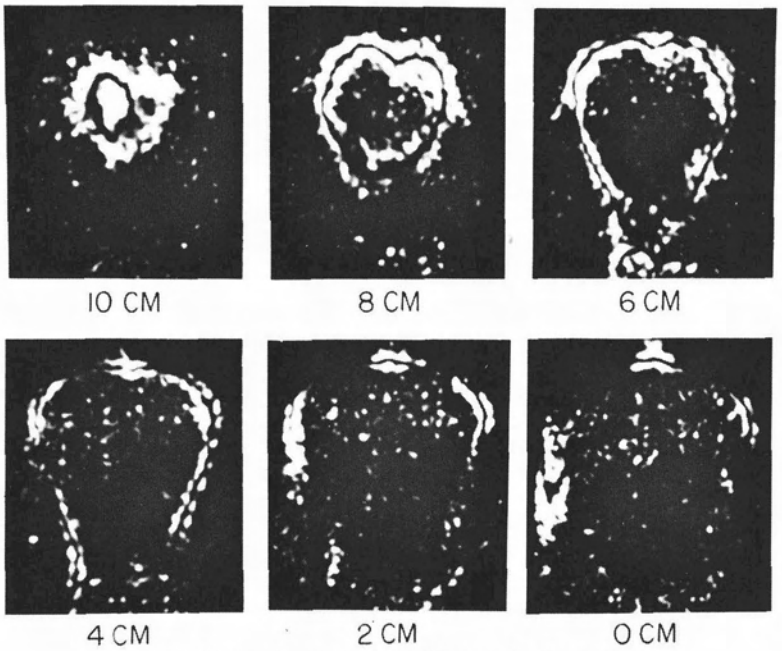

FIG. 12. Photos from a series of human-body contours.

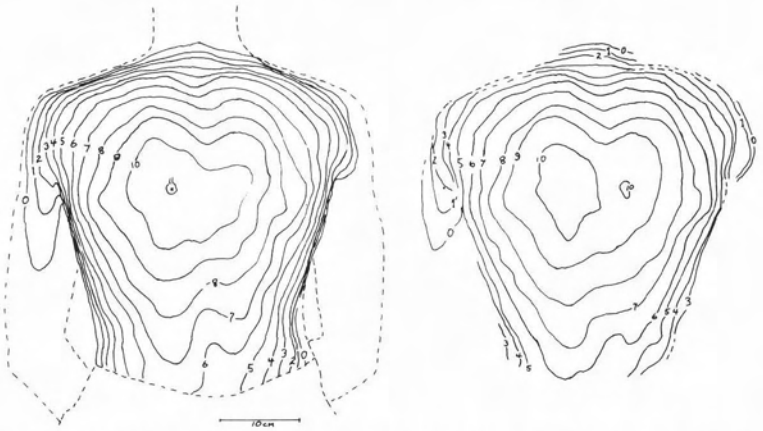

FIG. 13. *(Left)*: Classically prepared plot. *(Right)*: A composite of optically generated contours.

at a specific height) can be provided by a lens of variable focal length substituted for the final fixed focal-length lens shown in Figures 2 and 7. To satisfy Equation 3, the first transparency should be positioned so that its principal point coincides with the optical axis of the processing system. At the parallax setting for a specific contour, the focal length of the final lens is changed slightly so as to increase the magnification if the contour is lower than the reference level, or decrease the magnification for contours above the reference level. The zoom range of a lens used in this mode is roughly the ratio of the total height range to the reference height, or about 10 percent for photogrammetric work. This is a quite modest optical requirement. A less elegant but equally effective solution is differential enlargement of the photos recorded from the system. It is this second method which was used to generate the photos in Figure 12.

Another consideration is the requirement for coherent illumination and some of the problems involved with its use. All the work reported here was performed with light from a Mercury arc lamp, and sufficient coherence was attained by imaging the source through a 165 μm pinhole before collimation by a 150-mm focal-length lens. This provided illumination with sufficient coherence over a

small region of the transparency to perform the processing in a coherent domain, but not enough coherence to introduce any speckle in the system.

Over larger formats it may be necessary to use a laser source, but primarily due to the increased power attainable, rather than the need for more coherence. If used as a visual system, the color of the illumination makes a difference in eye fatigue. In comparison tests, the green Mercury light was found to be much more pleasing than a red Helium-Neon laser, especially over long periods of operation.

Thickness variations in the emulsions or the film support were not found to cause problems with these systems. It was, however, necessary to hold the transparencies quite flat, so that the image of one fell exactly on the other. On occasion it was necessary to sandwich the negatives between two glass plates to achieve the required flatness. In this instance a few drops of index matching fluid between the film and the plates prevented any artificial interference phenomenon. This was, in effect, a liquid gate often used in coherent processing. However it was never needed with glass-plate negatives which provided the necessary flatness.

Summary

The two basic systems presented here provide a rapid means of generating contours of equal elevation from a pair of vertical transparencies. The positive-negative system, with sufficient scene detail, provides a relatively moderate resolution capability, which includes fairly steep slopes. One disadvantage is that an intermediate copy or copies must be made to fairly exacting photographic requirements. It can, however, be used with totally incoherent light, even though coherent operation may greatly enhance the visibility of the contours.

The scatter-plate system uses transparencies directly from the camera, without intermediate processing. The performance on steep slopes falls off more rapidly than the first system, but the resolution attainable with low and intermediate slopes in the phase plate mode is competitive with the positive-negative system.

Currently these systems provide a potential for applications in close-range work where there is freedom to control the scene detail. The contours generated in the close-range example compare favorably with the classically prepared map. Accordingly, these systems offer a potential for the substantial reduction of time required for contour extraction without sacrificing too much in resolution.

Appendix

An analysis is outlined here to describe the characteristic contour width. The amplitude transmittance of each transparency is expressed as a sum of a bias term, c, and a scene structure term, f.

$$t_1(x_1,y_1) = c_1 + f_1(x_1,y_1)$$
$$t_2(x_2, y_2) = c_2 + f_2(x_2, y_2). \tag{19}$$

In the first transform plane, the bias term of the first transparency is blocked by an opaque spot. The block, which may be a more complex filter, is denoted as $B_1(\omega,\eta)$. What remains in the first Fourier plane is the product of B_1 with the transform of f_1, which is:

$$S_1(\omega,\eta) = B_1(\omega,\eta)\, F_1(\omega,\eta). \tag{20}$$

The inverse transform of this distribution is multiplied by $t_2(x, y)$ in the plane of the second transparency. However, one may skip directly to the second Fourier plane, because the product of two functions has a Fourier transform equivalent to the convolution of the individual transforms. The entire transform is then multiplied by the aperture function, $B_2(\omega,\eta)$. *Thus,*

$$S_2(\omega,\eta) = c_2\, F_1(\omega,\eta)\, B_1(\omega,\eta)\, B_2(\omega,\eta)$$
$$+ \left\{\left[B_1(\omega,\eta)\, F_1(\omega,\eta)\right]^* F_2(\omega,\eta)\right\} B_2(\omega,\eta). \tag{21}$$

The symbol * denotes convolution.

This equation shows the constraint that the block must be equal to or larger than the aperture, for only then will B_1B_2 be zero everywhere, eliminating the first term. If this condition is violated, large amounts of light from the first transparency are allowed to pass, obscuring the term of interest, which is the second term of Equation 21.

Denoting b_1 and b_2 as the transforms of the filter functions B_1 and B_2 and writing one transparency in terms of the other, the amplitude in the final image plane is written:

$$a(x, y) = b_2(x, y) *$$
$$\left\{f(x - p(x, y), y)\ \left[f(x,y) * b_1(x,y)\right]\right\}. \tag{22}$$

To predict the most likely value for the amplitude $a(x,y)$, one takes an ensemble average of the expression in Equation 22. The terms b_1 and b_2 are invariant in the averaging process, and b_2 may be brought outside of the average immediately. Explicitly writing the convolution with b_1 shows how the term

within the braces in the last equation is simplified by bringing all the terms into the integration. The bar denotes the ensemble average process:

$$\overline{a(x,y)} = b_2(x,y) * \iint \frac{\overline{f(x',y')\ f(x-p\ (x,y),\ y)}}{\overline{b_1(x-x',\ y-y')}}\ dx'\,dy' \quad (23)$$

Interchanging the order of averaging and integration, assuming that the sample function f is wide-sense stationary in the statistical sense, and ergodic[11], allows a simplification of Equation 23. The average may now be written in terms of the autocorrelation of f, defined as R(x,y). Thus, the previous equation reduces to

$$\overline{a(x,y)} = b_2(x,y)^* \left\{ [b_1(x,y)^*\ R(x,y)] \Big| \right. \\ \left. x = p(x,y),\ y = O \right\} \quad (24)$$

The convolution of b_1 with R occurs first, and then the substitution of $x = p(x,y)$ and $y = 0$ is made.

Acknowledgements

The authors would like to thank Mr. Robert McGivern of LaFave, Huntley, White, and McGivern, Rochester, New York, for preparing the contour map reproduced in the left half of Figure 13.

Part of this work was supported by the U. S. Army Engineering Topographic Labs Research Institute. One of us (A. W.) would like to thank Wild Heerbrugg Instruments, Inc. and the American Society of Photogrammetry for fellowship support provided in connection with this work.

References

1. A. F. DiPentima, "Automation in Photo Interpretation," *Photogrammetria*, 26:167-182, 1970.
2. Goldfischer and Vesper, "Automatic Stereo Perception of Aerial Photography by Means of Optical Correlation." Final technical report on contract DA-44-009-Eng-4966 prepared for U. S. Army GIMRADA, 1962.
3. R. R. Real, "An Approach to Data Processing of Stereo Photographs by Coherent Imaging," *Applied Optics*, 8:2, 411-417, 1969.
4. W. E. Chapelle, et al. "Automation in Photogrammetric Compilation," *Bendix Technical Journal*, 1:2, 1-13, 1968.
5. S. J. Krulikoski, et al. "Coherent Optical Parallel Processing," *Bendix Technical Journal*, 1:2, 59-65, 1968.
6. S. J. Krulikoski, et al. "Coherent Optical Mapping Techniques," Final Technical Report RADC-TR-70-62, May, 1970, AD No. 870942L.
7. Certain aspects of this system are quite similar to the Auto Stereo Profiler, described by T. A. Hughes, et al., "USGS Automatic Orthophoto System," *Photog. Eng.*, 37:10, 1055-1062, 1971.
8. J. W. Goodman, *Introduction to Fourier Optics*, McGraw-Hill, New York, 1968, p. 153.
9. J. M. Burch, "Interferometry with Scattered Light," *Optical Instruments and Techniques* (Oriel Press, 1969), p. 213-229.
10. D. C. Kowalski, "A Comparison of Optical and Electronic Correlation Techniques," *Bendix Technical Journal*, 1:2, 72-80, 1968.
11. W. B. Davenport and W. L. Root, *An Introduction to the Theory of Random Signals and Noise*, McGraw-Hill, New York, 1958, chapter 4.

Articles for Next Month

R. B. Forrest, Refraction compensation.
G. J. F. Holden and *L. Berlin*, Independent models and calculators.
J. H. Kreitzer and *B. Gilbertson*, Exposure for multispectral
D. Q. McDowell, Spectral distribution of skylight energy.
D. Q. McDowell and *M. R. Specht*, Spectral reflectance using aerial photographs.
D. C. Merchant, Calibration of air photo system.
G. L. Raines and *K. Lee*, Spectral reflectance measurements.
J. W. van Roessel and *R. C. de Godoy*, SLAR mosaics for Project RADAM.